J Mater Sci (2009) 44:3928–3935
DOI 10.1007/s10853-009-3526-4

Microstructural evolution in an ultralow-C and high-Nb bearing steel during continuous cooling

Yun Bo Xu · Yong Mei Yu · Bao Liang Xiao · Zhen Yu Liu · Guo Dong Wang

Received: 10 November 2008 / Accepted: 27 April 2009 / Published online: 24 May 2009

Abstract The microstructural evolution during continuous cooling has been investigated in an ultralow-C and high-Nb containing steel and compared to that of a traditional Nb–Mo pipeline steel. The deformation promotes the formation of fine-grained quasi-polygonal and acicular ferrite in coarse grain sized austenite. Lowering the austenite grain size leads to a loss in hardenability of austenite despite the fact that grain sizes of the final microstructure are refined. The high-Nb and Nb–Mo bearing materials have the nearly same effect on lowering the onset temperatures of transformation, but the former is somewhat faster in the progress of transformation due to an additional work-hardening effect. Thus, to obtain sufficient amounts of ultrafine-grained acicular ferrite, cooling rate must be increased to suppress the formation of high-temperature transformed products in high-Nb materials.

Introduction

Acicular ferrite, firstly reported by Smith et al. [1] in the early 1970s, has been widely accepted as one of the most attractive microstructures for the oil and gas pipeline steels because of its high strength and toughness potential [2–4]. Mo element is commonly added to pipeline steels in order to obtain this desired acicular ferrite structure through the suppression of high-temperature transformation products [5, 6], i.e., polygonal ferrite. However, for Mo-containing steels, there are also some inherent disadvantages such as high alloying cost, large mill load, and low production efficiency due to low temperature heavy deformation in non-recrystallization region of austenite. Thus, driven by economic benefits, some steel makers have recently adopted a new high-Nb microalloying technology in the development of high strength pipeline steels, which allows Nb content up to 0.1% in steels and using high-temperature processing (HTP) technology in rolling [7, 8]. This is mainly because that, the high lever of Nb in austenite is capable of promoting the acicular ferrite transformation from the undercooled austenite by restraining the formation of polygonal ferrite due to strong solute drag and precipitation pinning effect [9, 10]. In addition, the addition of Nb heightens austenite's non-recrystallization temperature through strongly retarding static and dynamic softening, thereby reducing flow stress and mill load greatly. This HTP-technology, as a feasible alternative to the conventional Mo-alloying method in high grade pipeline steels [11], is showing a developing tendency and prospect in a variety of applications. There are, however, few reports on the microstructure and mechanical properties of high-Nb HTP steels and the comparisons between this material and traditional Nb–Mo pipeline steel. Also, in HTP steels the transformation behavior of acicular ferrite and their effects on the combination properties are detailedly not known. Therefore, it is necessary to investigate the microstructure evolution of HTP steels, especially for their transformations behaviors, and how those transformations are affected by changes in alloy additions and processing parameters.

Y. B. Xu (✉) · B. L. Xiao · Z. Y. Liu · G. D. Wang
State Key Laboratory of Rolling Technology and Automation, Northeastern University, P.O. Box 105, Shenyang 110004, People's Republic of China
e-mail: xuyunbo@mail.neu.edu.cn

Y. M. Yu
Mechanical Engineering School, Shenyang University of Chemical Technology, Shenyang 110142, People's Republic of China
e-mail: yongmei_yu@126.com

A continuous cooling transformation (CCT) diagram is a useful way to better understand the transformation behavior of a material as a function of thermomechanical processing parameters. In this study, the effect of microstructure, hot deformation and cooling variables on phase transformation of the ultralow-C and high-Nb bearing HSLA steel and some significant differences compared to the traditional Nb–Mo steel are presented. The aim of this study is to clarify the formation of the acicular ferrite dominated microstructure in this high-Nb and Mo-free material by investigating the effects of alloy additions and hot deformation on the CCT behaviors.

Material and experimental procedures

Material

The high-Nb and traditional Nb–Mo bearing HSLA steels used in this study were, respectively, prepared in a 120 kg vacuum induction melted furnace. Table 1 shows the chemical composition of the present two steels. Notably, in steel A the Nb content is 0.1% and there is no Mo addition, i.e., it is significantly different from that of steel B with predominantly Mo microalloying. In addition, by lowering carbon content, i.e., less than 0.03 weight % and using Ti/N treatment where sufficient Ti was present to combine with N in the steel, large amounts of Nb can be dissolved in austenite during reheating. C and S were measured by CS-244 Infrared Analyzer, N and O were measured by PC-T36 Nitrogen/Oxygen Determinator and the other elements were measured by ICP Direct-Reading Spectrometer.

Experimental procedures

In smelting and casting, electromagnetic stirring were employed to significantly reduce and micro- and macro-segregation and improve homogeneity. The cast ingots were forged into square billets of 100 mm thickness and 100 mm width. The austenitized and homogenized treatments were done at 1200 °C for 1–3 h, and then these square billets were rolled into the 10–11 mm thick plates using a laboratory hot rolling mill. Standard cylindrical specimens with initial heights of 15 mm and initial diameters of 8 mm were machined from the plates with the specimen axes parallel to the plate transverse direction. In order to examine microstructural detail, laboratory tests were conducted on a Gleeble 2000 thermomechanical simulator including austenite grain growth, single and double hit as well as CCT tests. The austenite grain growth tests were carried out to determine reasonable austenitization conditions for subsequent deformation and transformation studies that require different initial austenite grain sizes. In this study, cylindrical specimens of 8 mm diameter and 15 mm length were heated at 20 °C/s to reheating temperatures in the range of 1000–1200 °C followed by holding for 3 min before quenching to reveal the prior austenite microstructure using etching and optical microscopy. The average linear intercept grain size was measured for at least 10 random fields using computer aided image analysis to describe the effect of initial grain size on transformation behavior.

CCT tests with and without deformation were performed to measure the austenite decomposition with dilatometry and metallographically analysis as a function of cooling rate and initial austenite microstructure. Following austenitization, cylindrical specimens of 10 mm diameter and 15 mm length were cooled at 10 °C/s to a designated temperature, i.e., 900 °C, where they were held for 30 s for temperature homogenization. Subsequently, the specimens used for no-deformation test were directly cooled to room temperature,and the others used for hot deformation test were compressed with the strain of 0.2 or 0.4 and then cooled to room temperature,where the cooling rates was controlled to vary in the range of 1–40 °C /s.

A combination of the optical microscopy and dilatometric analysis and transmission electron microscopy (TEM) were employed in determining the microstructures of the specimens. The specimens for metallographic analysis were mechanically polished and etched with a 3% Nital solution, and then observed using optical microscopy. For TEM observation, the thin foils were mechanically thinned from 300 to 50 μm, and then electropolished by a twin-jet electropolisher in a solution of 10% perchloric acid and 90% acetic acid. The thin foil specimens were observed using H-800 TEM with 200 kV.

Results and discussion

Effects of initial grain size and prestrain amount on microstructure after transformation

This acicular ferrite is defined as a low-carbon bainitic structure with lath characteristic that forms during cooling

Table 1 Chemical composition of the tested steels (wt%)

Steel	C	Si	Mn	Cu	Ni	Nb	Mo	Ti	Al	N
A	0.024	0.17	1.49	0.26	0.15	0.10	–	0.01	0.027	≤0.0036
B	0.05	0.21	1.58	0.12	0.16	0.05	0.19	<0.01	0.025	≤0.0040

through a combined mode of diffusion and shear transformation at a temperature range slightly higher than upper bainite. This microstructure containing high density dislocations and a great deal of substructure due to its relatively low transition temperature exhibits a superior strength and toughness combination and thus widely accepted in the manufacturing and application of pipeline steels. However, the acicular ferrite observed in optical micrographs is not isolated but commonly combined with polygonal ferrite, quasi-polygonal ferrite and bainitic ferrite, etc., as shown in Figs. 1 and 2.

Figure 1 shows the optical micrographs for the tested steel at different prestrains. The transformed microstructure without deformation is mainly bainitic ferrite and a fairly small amount of acicular ferrite. The corresponding transformed microstructures in deformed conditions, comprising acicular ferrite and quasi-polygonal ferrite, are markedly different in shape and volume fraction of each phase from those in undeformed cases. The acicular ferrite matrix is characterized by the non-equiaxed ferrite, which has various size grains distributed in a random manner and the sizes are reduced with increasing the strain. It is also found that the deformation promotes the formation of acicular ferrite and quasi-polygonal ferrite.

The effect of initial grain size on transformed microstructure is illustrated in Fig. 2 for a strain of 0.4 and a cooling rate of 10 °C/s. The acicular ferrite dominant microstructure can be obtained for all initial austenite grain sizes referred here. For the grain size of 65 μm, the transformed products seemingly form at relatively low temperatures, and it possesses a great deal of irregular bainitic and acicular ferrite grains in shape and size and distributed in a chaotic manner with random orientations. Small amounts of coarse quasi-polygonal ferrite can also be observed. As the

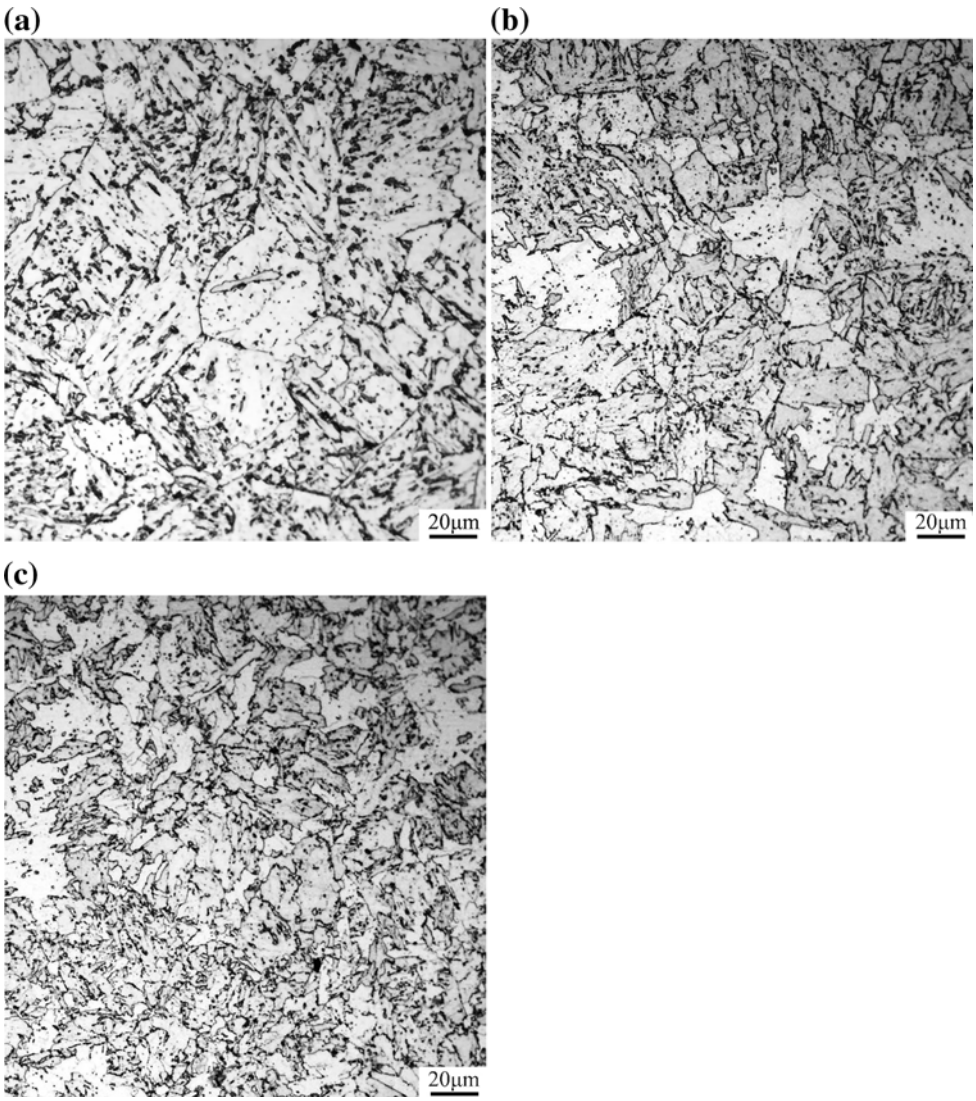

Fig. 1 Optical micrographs for the tested steel at different strains ($d_\gamma = 65$ μm; $v_c = 5$ °C/s): **a** $\varepsilon = 0$; **b** $\varepsilon = 0.2$; and **c** $\varepsilon = 0.4$

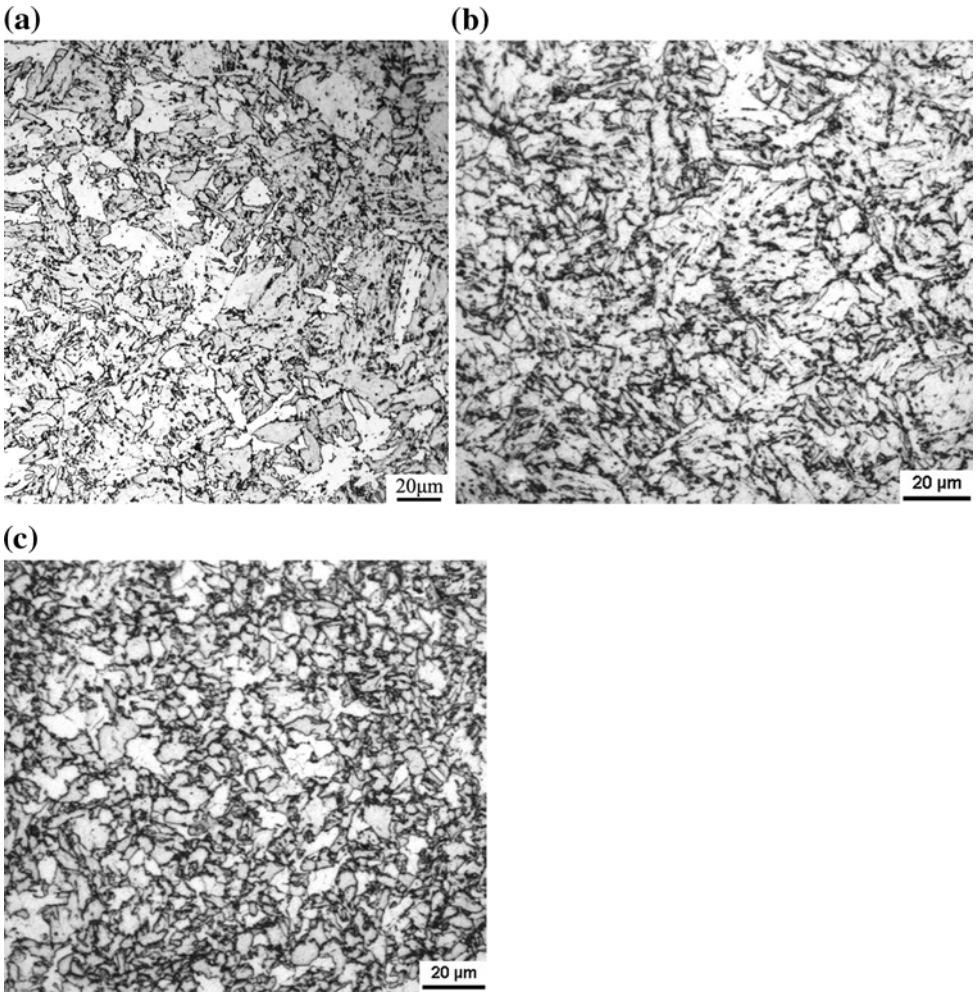

Fig. 2 Optical micrographs for the tested steel at different initial austenite grain sizes ($\varepsilon = 0.4$; $v_c = 10$ °C/s): **a** $d_\gamma = 65$ μm; **b** $d_\gamma = 43$ μm; and **c** $d_\gamma = 11$ μm

prior austenite grain size is reduced to 43 μm from 65 μm, the volume fraction of quasi-polygonal ferrite increases and bainitic ferrite can still be seen in some areas. For the lower austenite grain size of 11 μm, a significantly elevated proportion of equiaxed ferrite is present in the final microstructure, and their sizes are refined greatly. Thus, it can be seen that, austenite decomposition kinetics strongly depends upon the prior austenite condition such as grain size and retained strain that appears just before the start of the transformation. Reducing prior austenite grain size can give rise to the larger number of favorable nucleation sites, hence enhance greatly nucleation rate and promote the refinement of the final microstructure.

These results can be further explained from the point of view of the theory of interface mobility control transformation as follows. Assuming that the velocity (v) of the γ/α interface is proportional to the deviation of Gibbs free energy caused by the finite interfacial mobility $\left(\Delta G_{\mathrm{m}}^{\mathrm{int}}\right)$, it is then described by the following expressions

$$v = M_0 \exp\left(-\frac{Q}{RT}\right)\Delta G_{\mathrm{m}}^{\mathrm{int}} \tag{1}$$

$$\Delta G_{\mathrm{m}}^{\mathrm{int}} = \Delta G_{\mathrm{m}}^{\mathrm{tot}} - \Delta G_{\mathrm{m}}^{\mathrm{dif}} - \Delta G_{\mathrm{m}}^{\mathrm{sd}} - \Delta G_{\mathrm{m}}^{\mathrm{pre}} \tag{2}$$

$$\Delta G_{\mathrm{m}}^{\mathrm{tot}} = \Delta G^{\gamma\to\alpha} = \Delta G_{\mathrm{chem}} + \Delta G_{\mathrm{def}} \tag{3}$$

$$\Delta G_{\mathrm{def}} = 0.5Gb^2\rho V_{\mathrm{m}} \tag{4}$$

where R is the gas constant, T the temperature, Q the activation energy for atomic motion at the interface, M_0 the pre-exponential factor, and $\Delta G_m^{\mathrm{tot}}$ the total driving force for the γ/α transformation. In the case of transformation from deformed austenite, the total driving force $\Delta G^{\gamma\to\alpha}$ is expressed as the summation of chemical driving force ΔG_{chem} and the additional driving force arising from the stored energy of deformationΔG_{def}, G the shear modulus of Fe and $b$the Burgers vector of dislocation, ρ the dislocation density, and V_{m} the molar volume of the matrix. $\Delta G_{\mathrm{m}}^{\mathrm{dif}}$, $\Delta G_{\mathrm{m}}^{\mathrm{sd}}$ and $\Delta G_{\mathrm{m}}^{\mathrm{pre}}$ are the Gibbs energy dissipation due to the solute drag, the diffusion in the matrix ahead of interface and the pinning effect of precipitation particle. From these equations, it can be seen that, although sufficient solute Nb segregated in phase interface can lower the velocity of the γ/α interface through the increase of $\Delta G_{\mathrm{m}}^{\mathrm{sd}}$ [9], raising the strain would lead to the increase in dislocation density ρ

and deformation stored energy ΔG_{def}, thus elevating the transformation driving force and promoting the moving of phase interface. This is in accordance with the metallorgraphical results observed in Fig. 1. That is to say, with increasing strain, a microstructural change from the bainitic ferrite to acicular and massive ferrite appears in the final transformation products.

The other important parameter in the γ/α transformation kinetics is the effective grain boundary area in austenite S_{v}, which would determine ferrite nucleation site density. Adopting the equiaxed and spherical geometry for undeformed austenite grain, the prior austenite grain boundary per unit volume, S_{v0}, can be calculate by $2/d_{\gamma}$ [12], where d_{γ} is austenite grain size. When deforming below the nonrecrystallization temperature, the austenite grains are elongated and there is an increase of the specific grain boundary area. This causes an increase of nucleation site density. The same effect is attributed to the dislocations, deformations bands and twins that can also form during deformation. An effective boundary area can be defined by considering all these effects together, as shown in the following equation [13].

$$S_{\text{v}} = q \cdot S_{\text{v0}} + S_{\text{vdb}} = q \cdot S_{\text{v0}} + \text{A} \cdot \varepsilon_{\text{a}} + \text{B} \tag{5}$$

where q is the ratio of the grain boundary area of pancaked austenite after deformation corresponding to that of equiaxed austenite prior to deformation, being considered as a function of strain. ε_{a} is the accumulated strain in nonrecrystallization region, A and B are the constants. In the present case, there is a large increase of effective grain boundary area for smaller austenite grain sizes, for example, $d_{\gamma} = 43$ μm or $d_{\gamma} = 11$ μm in Fig. 2. Even assuming austenite grain is equiaxed, that is, not taking the effect of deformation into account, the S_{v0} value varies from 31 to 181 mm^{-1} when decreasing the austenite grain size from 65 to 11 μm. As a consequence, lowering the austenite grain sizes leads to the occurrence of more mounts of transformation products formed at somewhat higher temperatures. The other common feature of these microstructures is an apparent refinement of grain size with reducing austenite grain size. This is also attributed to the increase of effective grain boundary area acting as nucleation site, when austenite grain size is greatly refined.

Continuous cooling transformation diagram

The static and dynamic CCT diagrams for different prior austenite grain sizes are done using the thermal dilation method and the aforementioned microstructural observation, as illustrated in Fig. 3. The major transformation curves of the tested steels almost lie in the temperature range from 470 to 690 °C in undeformed samples, and from 490 to 790 °C in deformed samples, where initial grain sizes are ranged from 11 to 65 μm. In these temperature ranges, the formed microstructures may include acicular ferrite, polygonal ferrite, quasi-polygonal ferrite and bainitic ferrite. In the static CCT diagram (Fig. 3a), the transformed microstructures contain bainitic ferrite, and a small amount of acicular ferrite and quasi-polygonal ferrite, and polygonal ferrite is avoided in the tested cooling rate range. Figure 3b, c and d are the dynamic CCT diagrams at the prior strain of 0.4 and their initial austenite grain sizes are 65, 43 and 11 μm, respectively. It can be observed that, for initial grain size of 65 μm, the starting temperatures of acicular ferrite and/or quasi-polygonal ferrite in deformed samples ($\varepsilon = 0.4$) are higher than that of undeformed ones by 10–20 °C. With the decrease of initial austenite grain size, the corresponding transformation curves gradually move toward the top left corner, the nonisothermal austenite-polygonal ferrite transformation is also enhanced, and especially at initial grain size of 11 μm bainitic ferrite is completely suppressed for all applied cooling rates.

As stated above, the acicular ferrite grain can be significantly refined by adjusting austenite state such as increasing prior strain and decreasing initial austenite grain size. But, on the other hand, the high-temperature transformed products, i.e., polygonal ferrite, etc., may form at a faster rate and present in the final microstructure at a lager volume fraction. This is not expected because the increase of polygonal ferrite not containing high density dislocation would impair strength and toughness of steels. Therefore, it is necessary to ensure enough amounts of acicular ferrite to form by strengthening the subsequent cooling. For example, in the high-Nb steel, when $\varepsilon = 0.4$ and $d_{\gamma} = 43$–65 μm, the cooling rate should be at least higher than 5 °C/s, and with decreasing initial grain size, the value should be higher.

Comparisons between high-Nb material and traditional Nb–Mo pipeline steel

The comparison of optical micrographs between high-Nb steel (steel A) and traditional Nb–Mo X70 steel (steel B) at different cooling rates is shown in Fig. 4. At the cooling rate of 5 °C/s, the polygonal ferrite, quasi-polygonal ferrite and acicular ferrite dominate the microstructures of the two steel, and there is no essential difference in morphology and structure type, except that grain sizes of steel A are smaller. When cooling rate is heightened to 20 °C/s, the transformed microstructure of steel A is mainly quasi-polygonal ferrite, acicular ferrite and small amounts of polygonal ferrite, and their sizes are further refined. Figure 5 is the representative TEM micrographs of fine-grained quasi-polygonal and acicular ferrites in the ultra-low-C and high-Nb steel. The corresponding transformed

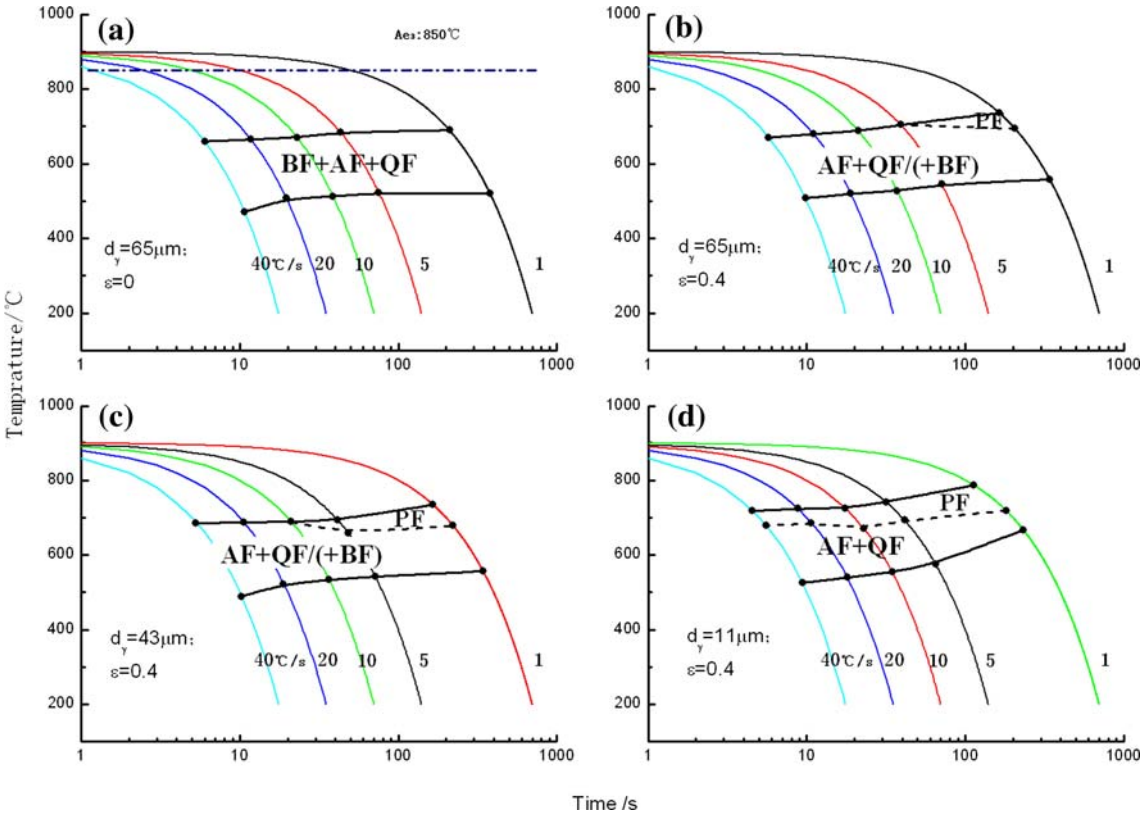

Fig. 3 CCT diagrams of steel A in undeformed and deformed conditions (*BF* bainitic ferrite, *AF* acicular ferrite, *PF* polygonal ferrite, *QF* quasi-polygonal ferrite): **a** $d_\gamma = 65$ μm, $\varepsilon = 0$; **b** $d_\gamma = 65$ μm, $\varepsilon = 0.4$; **c** $d_\gamma = 43$ μm, $\varepsilon = 0.4$; and **d** $d_\gamma = 11$ μm, $\varepsilon = 0.4$

microstructures of steel B (Fig. 4), comprising acicular ferrite and quasi-polygonal ferrite, are evidently different in shape from the former. Some acicular ferrites continue to grow up along the particular direction and start to exhibit the acerose lath characteristic, and additionally, the quasi-polygonal ferrite has various size grains distributed in a random manner throughout the matrix. The difference of transformation products between the two steels is related to the level of austenite work-hardening during hot deformation. The result in Fig. 6 indicates that, at $\varepsilon = 0.4$, all the stress values of steel A are higher than that of steel B by approximately 19–35 MPa in the range of 900–1100 °C. Equation 6 gives the relationship between flow stress and dislocation density, where σ and σ_y are the flow stress and yield stress, respectively, at the deformation temperature, M is Taylor factor and α the constant.

$$\rho = \left(\frac{\sigma - \sigma_y}{M\alpha\mu b}\right)^2 \tag{6}$$

It can be seen that, with the increase of the flow stress, the dislocation density and deformation stored energy (see Eq. 4) increase, the driving force and site density for nucleation are elevated, and hence the grain sizes of the transformed acicular ferrite and quasi-polygonal ferrite are greatly refined, especially at a relatively high cooling rate. That is to say, compared to traditional Nb–Mo X70 steel, under reasonable rolling and cooling conditions, the high-Nb steel can obtain a uniform and ultrafine acicular ferrite grain in sizes, which is a very attractive microstructure for high grade pipeline steels. Noting that, cooling rate must be increased to suppress the formation of high-temperature transformation products.

On the other hand, the transformation times (t) for steel A are found to be shorter than that of steel B, though there is no significant difference in transformation starting temperatures (T_s) of both steels, as shown in Fig. 7. This result indicates that both steels have the nearly same effect on lowering the onset temperatures of transformation, but the progress of transformation is faster in high-Nb steel compared to Nb–Mo steel at various cooling rates. Effect of dissolved Nb on γ/α transformation is already well known. For the role of precipitation, some authors [14, 15] believe that the precipitates formed in austenite, particularly those precipitates which form at temperatures approaching the transformation, can pin the interphase interface during transformation. In this study, whether Nb is in solution or Nb is present as strain induced precipitates (particularly at relatively low cooling rates), high-Nb material exhibits the strong effect of retarding the transformation relative to

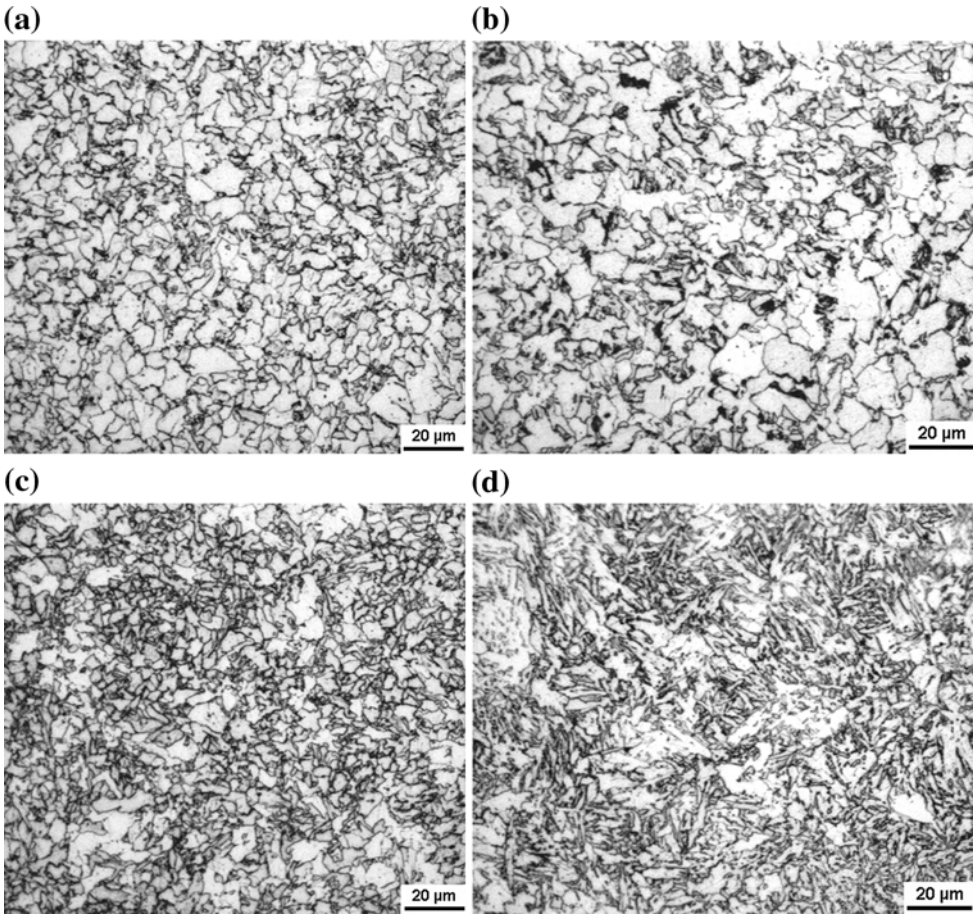

Fig. 4 Optical micrographs for the tested steel A and B at different cooling rates ($\varepsilon = 0.4$; $d_\gamma = 11$ μm): **a** Steel A, 5 °C/s; **b** Steel B, 5 °C/s; **c** Steel A, 20 °C/s; and **d** Steel B, 20 °C/s

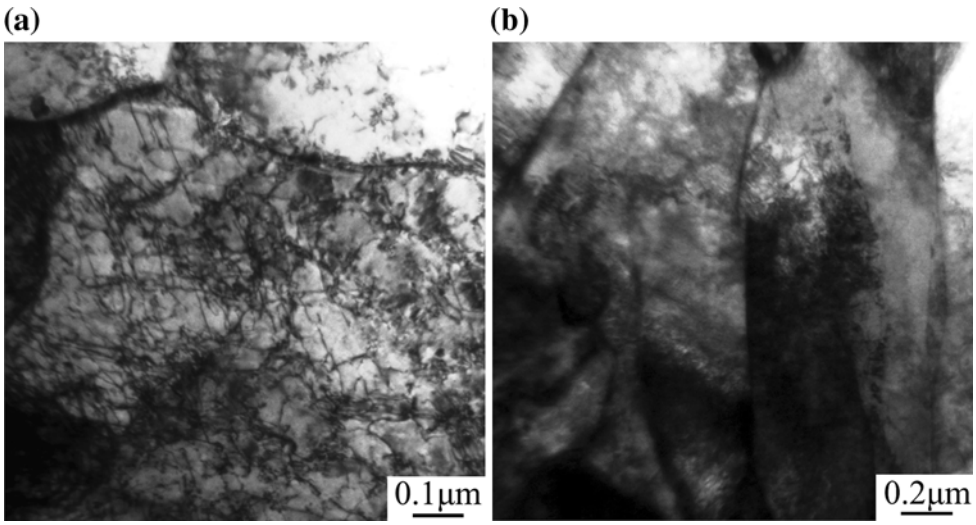

Fig. 5 TEM micrographs showing: **a** quasi-polygonal ferrite containing high density of dislocations and **b** acicular ferrite with fine lath morphology in the high-Nb steel

nucleation, and hence T_s is pushed toward the relatively low temperatures. However, the retarding effect of Nb on the progress of transformation in high-Nb steel seems to be somewhat lower than that of Nb–Mo steel, which is of course related to higher deformation stored energy in the former. Additionally, the relatively high Mn content in steel B is also responsible for this sluggish transformation kinetics to a certain extent. It is well-known that Mn in steels could act as the elements to broaden the austenite region. Thus, the relatively high levels of manganese will further suppress the formation of high-temperature products through stabilizing the austenite and solute drag effect.

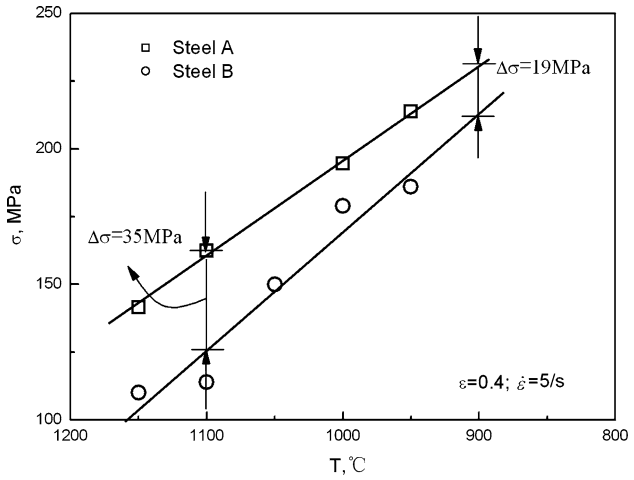

Fig. 6 Comparison of the flow stress (σ) of both steels at various deformation temperatures

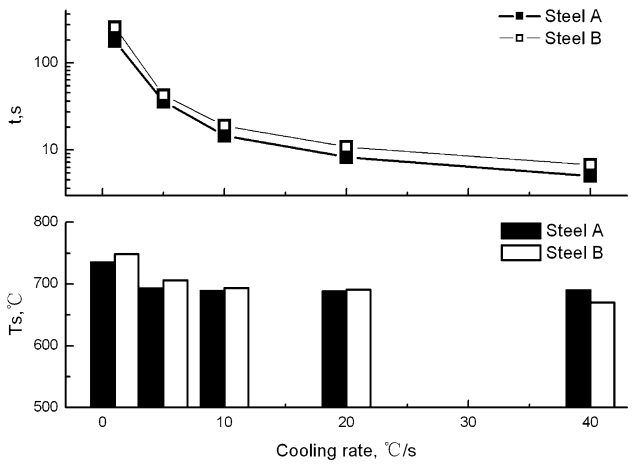

Fig. 7 Comparison of the times (t) and onset temperatures (T_s) of transformation in both steels at various deformation temperatures

Conclusion

In this study, the effects of initial grain size, prestrain amount, and cooling rate on the CCT behavior of an ultralow-C and high-Nb bearing steel were investigated. It has been found that the transformed products and their grain size of the high-Nb steel are strongly dependent on prior austenite conditions such as initial grain size and retained strain, as well as cooling parameters after hot deformation. For coarse grain sized austenite, the onset temperatures of acicular ferrite and/or quasi-polygonal ferrite in deformed samples are higher than that of undeformed ones by 10–20 °C. Lowering the austenite grain size leads to an increase of the volume fraction of new phases formed at somewhat higher temperatures and their sizes are refined greatly. The overall transformation occurs in the temperature range from 470 to 690 °C in undeformed samples, and from 490 to 790 °C in deformed conditions, at initial grain sizes ranging from 11 to 65 μm. The comparison between high-Nb and Nb–Mo bearing materials indicates that both have the nearly same effect on lowering the onset temperatures of transformation, but the former is somewhat faster in the progress of transformation at various cooling rates due to an additional work-hardening effect. Thus, to obtain sufficient amounts of ultrafine-grained acicular ferrite, cooling rate must be increased to suppress the formation of high-temperature transformation products in high-Nb materials.

Acknowledgements This study was financially supported by the National Natural Science Foundation of China under contract No. 50504007 and the National Key Project of Scientific and Technical Supporting Programs (No. 2007BAE51B07). This study also was supported by Benxi Iron and Steel Corp., China.

References

1. Smith YE, Coldren AP, Cryderman RL (1972) Toward improved ductility and toughness. Climax Molybdenum Company (Japan) Ltd, Tokyo
2. Kim YM, Kim SK, Lim YJ et al (2002) ISIJ Int 42:1571
3. Smith Y, Coldren A, Cryderman R (1976) Met Sci Heat Treat 18:59
4. Zhao MC, Shan YY, Xiao FR et al (2003) Mater Lett 57:1496
5. Kong JH, Zhen L, Guo B et al (2004) Mater Des 25:723
6. Tang ZH, Stumpf W (2008) Mater Charact 59:717
7. Hulka K, Bordigon P, Gray M (2006) Microalloy Technol 6:1
8. Stalheim DG, Barnes KR, Mccutcheon DB (2006) Microalloy Technol 6:15
9. Suehiro M, Liu Z-K, Ågren J (1996) Acta Mater 44:4241
10. Suehir M (1998) ISIJ Int 38:547
11. Siciliano F Jr, Jonas JJ (2000) Metall Mater Trans A31:511
12. Bengochea R, Lápez B, Gutierrez I (1999) ISIJ Int 39:583
13. Kvackaj T, Mamuzic I (1998) ISIJ Int 38:1270
14. Subramanian SV, Zeng X, Collins LE et al (1993) In: Asfahani R, Tither G (ed) Proceedings of international symposium on 'Low carbon steels for the 90's'. TMS, Pittsburgh
15. Sellars CM (1985) In: Gray JM et al (ed) Proceedings of international conference on 'HSLA steels: metallurgy and applications'. Beijing